LAMONT-DOHERTY GEOLOGICAL OBSERVATORY
OF COLUMBIA UNIVERSITY
PALISADES, NEW YORK 10964

The Use of Pulse Shapes in Seismic Body Waves, to Determine the Nature of the Seismic Source

Semi-Annual Report No. 2

Contract F49620-77-C-0098

1 April 1978

Sponsored by
Advanced Research Projects Agency (DOD)
ARPA Order No. 3291
Monitored by AFOSR Under Contract # F49620-77-C-0098

Semi-Annual Report No. 2

ARPA order number:	3291
Program code number:	7F10
Contractor:	Trustees of Columbia University
Effective date of contract:	1 April 1977
Contract expiration date:	30 September 1978
Amount of contract:	$61,992
Contract number:	F49620-77-C-0098
Principal investigator:	Prof. Paul G. Richards 914-359-2900 x 389
Program manager:	Prof. Paul G. Richards 914-359-2900 x 389
Short title:	Pulse Shapes and the Nature of the Seismic Source

Sponsored by
Advanced Research Projects Agency (DOD)
ARPA Order No. 3291
Monitored by AFOSR Under Contract # F49620-77-C-0098

SUMMARY

Over the past six months, we have completed a major data analysis investigation of five large aftershocks ($4.0 < m_L < 4.9$) of the August 1, 1975 Oroville, California earthquake. These events were each recorded by eight or more SMA1's at hypocentral distances of 8 to 20 km. The measurement and analysis of the energy flux in the shear wave arrivals, as suggested in the last semi-annual report, has been shown to provide a significant improvement in the estimation of source dimension, as well as to permit quantitative estimates of the radiated seismic energy and the apparent stress. Displacement pulse shapes, spectra and energy flux pulse shapes vary in a systematic fashion over the focal sphere, although these variations differ somewhat from the variations predicted by the circular models discussed in the last semi-annual report. In order to evaluate and resolve these differences, we have derived an asymmetric healing model from an extension of our previous modelling work, which retains the "pseudo-dynamic" character of the circular models. As the conclusions for the analysis of the Oroville data depend on the results of our modelling, on which we have only just begun work, we will delay discussion of those results to the September 1978 semi-annual report. In this report, we will discuss the theoretical motivation and analysis for these "pseudo-dynamic" models of rupture, both as functional constraints for the rupture motion and as a general framework for modelling considerations. We have included as an appendix a translation from the Russian of part of a recent book by B. V. Kostrov on source theory, which provides an analytic framework for consideration of the non-uniqueness of source modelling. Our discussion is summarized in the following two paragraphs.

I.- The inverse problem of seismic source theory, using a finite number of far-field observations, is a seriously non-unique problem. It is necessary then to seek to reduce this non-uniqueness by constraining the class of rupture models to be dynamically consistent, both in their nucleation and in their healing. As the far-field wave-forms depend on an integration over the rupture area of the particle velocity, we have derived specific analytic forms for the particle velocity in these two phases, i.e., the nucleation (or self-similar) phase and the healing (or transitional) phase. In our specification, the interaction of these two phases on the fault perimeter produces a realistic stopping behavior, allowing us to model earthquakes whose body wave spectra show a wide range of spectra falloffs and high frequency structure.

II.- The resulting general model is approximately correct in its radiation efficiency, enabling us to use the time histories of the seismic energy flux, as well as the time-integrated energy flux, as realizable model constraints. The radiated seismic energy is strongly focussed in the direction of rupture propagation for a model with a significant unilateral component of rupture. Our asymmetrical model (hereafter referred to as the A-model) details the transition from the (degenerate) circular models (the D- and M-models discussed in the September 1977 semi-annual report) to unilateral models of rupture. This general model will do much to aid the interpretation of earthquakes whose pulse shapes and spectra vary strongly over the focal sphere.

INTRODUCTION

It is useful to begin by considering the non-uniqueness of the inverse problem of seismic source theory. Formulated in terms of the far-field approximation, this inverse problem requires the solution of the inverse triple-transform,

$$\Delta\dot{\underset{\sim}{u}}(\underset{\sim}{\xi},t) = \frac{1}{8\pi^3} \iiint F(\underset{\sim}{k},\omega) e^{i\omega t + i\underset{\sim}{\xi}\cdot\underset{\sim}{k}} dk_1\, dk_2\, d\omega \qquad (1)$$

where $F(\underset{\sim}{k},\omega)$, the triple-transform of the distribution of the slip velocity on the rupture area, is determined within the domain

$$k_1^2 + k_2^2 \leq \frac{\omega'^2}{\beta^2}, \qquad (2)$$

where ω' is the highest resolvable frequency, from measurements of the Fourier transforms of the far-field pulse shapes in all directions. Kostrov (1975) [see Appendix] has demonstrated that the solution of this inverse problem is non-unique or "instable"; i.e., even with a sufficiently sampled transform, $F(\omega,\underset{\sim}{k})$, obtained from a dense set of far-field observations, one cannot distinguish the dimensions of the rupture area without adducing constraints on the class of functions, $\Delta u(\underset{\sim}{\xi},t)$, which describe the slip at the source beyond inclusion in the class L_2. Although the assumption of an unreversed slip reduces this instability, the inverse problem is still non-unique under this constraint. This result also implies the possibility of fitting any particular class of simple functions describing the seismic source to obtain as close a fit as desired to a set of observations without correctly modelling the motion

at the focus. For a finite set of actual observations, this non-uniqueness assumes an overwhelming importance, such that the use of a particular "source model" (i.e., Brune, 1970; Savage, 1972; Madariaga, 1976; etc.) becomes the most important decision in determining the necessary source parameters of fault dimension and stress drop. It is this choice of source models which this report seeks to address in a heuristic fashion, in an effort to motivate the use of dynamically consistent models of rupture.

Our "pseudo-dynamic" models are designed to incorporate two basic physical considerations. First, the rupture is presumed to grow in a causal fashion from a point (the hypocenter), such that the crack tip acts as an energy focus. We presume that the dynamics of the crack growth are adequately described by an elliptical slip distribution, where the particle velocity is a maximum as the rupture front passes and slows asymptotically to a constant value until the rupture begins to heal. Second, the healing itself is approximately causal, such that the onset of healing propagates from a stopping event, or from a locus of stopping events, into the interior of the rupture area at a finite velocity, presumably the compressional wave velocity. The healing is further assumed to be monotonic, i.e., we do not attempt to incorporate break-out phases (resulting from the interaction of the rupture front with a free surface; Burridge and Halliday, 1971), and we assume that in the presence of a finite frictional stress, the rupture will heal without reversal of slip.

This heuristic approach to kinematic modelling naturally divides the particle velocity for any point on the rupture area into two distinct phases, which we will refer to as the nucleation phase and the healing phase. The following two sections will be taken up in motivating the specific analytic forms for these phases which we use to generate our synthetic body wave pulse shapes.

NUCLEATION

During the nucleation phase, the particle motion is assumed to be purely elliptical, i.e., described by

$$\left.\begin{aligned} \Delta u_n(\underset{\sim}{\xi},t) &= A(\underset{\sim}{\xi})(t^2-T_r^2(\underset{\sim}{\xi}))^{\frac{1}{2}} \\ \Delta \dot{u}_n(\underset{\sim}{\xi},t) &= A(\underset{\sim}{\xi})t/(t^2-T_r^2(\underset{\sim}{\xi}))^{\frac{1}{2}}, \end{aligned}\right\} \quad t > T_r(\underset{\sim}{\xi}) \tag{3}$$

where $T_r(\underset{\sim}{\xi})$ is the arrival time of the rupture front and $A(\underset{\sim}{\xi})$ is a velocity which depends on the effective stress, τ_e, and the rupture velocity, v, approximately as $A(\underset{\sim}{\xi}) \approx v\tau_e/\mu$ (Dahlen, 1974). Figure 1 shows the resulting particle velocity as a function of time for a representative point on the fault. It is necessary to point out that this representation, *while suitably general, does not* incorporate any of the complexities such as diffraction effects, introduced by abrupt changes of the rupture velocity (other than stopping) or variations in time of the dynamic frictional stress. In our implementation of eq. 3, we presume the loading stress to be approximately homogeneous and use a constant rupture velocity, thereby fixing $A(\underset{\sim}{\xi}) = A(0)$, where A(0) is the particle velocity at the hypocenter.

It is also important to note that while eq. 3 represents a dynamically consistent slip distribution for a subsonically growing rupture (Richards, 1973), it may also be appropriate for describing an approximate transonic model, where the rupture velocity of the plane strain component lies between the shear wave and compressional wave velocity, while the anti-plane strain component is less than or equal to the shear wave velocity (Burridge, 1973). Elliptical models with transonic rupture velocities may be simply programmed by a minor

extension of the code we are presently using to compute synthetic pulse shapes. Theoretical investigations of transonic rupture growth are comparatively recent, however, and more work must be done to insure we can properly incorporate these results before any modelling is attempted.

The presence of the half-order singularity in slip velocity is handled in a computationally efficient fashion, as described in the September 1977 semi-annual report. In actual materials, the peak particle velocity is bounded due to the finite yield strength of the rock, since this is the upper bound for the stress concentration at the crack tip (Andrews, 1976, 1977). Thus, a more realistic form for the particle velocity would be a smoothed version of Figure 1, such that it reflected this boundedness. However, as the far-field pulse shape is obtained by an integration over the rupture area, a bounded version of eq. 3 would produce approximately the same result, so that our simple analytic form is adequate.

HEALING

The healing phase represents a transition from the elliptical slip or nucleation phase to the static final offset. We presume the onset of healing to be a diffraction effect, propagating from a locus of stopping events (i.e., the slowing or stopping of the rupture front) into the interior of the fault (Madariaga, 1977; Achenbach, 1978). In our circular healing model, discussed in the September 1977 report, this locus was a circle which the rupture front reached simultaneously at all azimuths. This unphysical azimuthal behavior produced anomalous pulse shapes, spectra and energy flux within the cone $\frac{v}{c} \sin\theta < .2$. Snapshots of the particle displacement during the rupture growth

and healing are shown in Figure 2, with the part of the fault which is healing shown darkened. The analytic form used for this healing phase, (eq. 20b, September 1977 report)

$$\Delta u_h(r,t) = A(0)\ (t^2-\nu(r)(t-T_s(r))^2 - \frac{r^2}{v^2}\ )^{\frac{1}{2}} \qquad T_s(r) < t < T_h(r) \qquad (4)$$

where $T_s(r)$ is the arrival time of the P-wave generated at the perimeter of the fault, was obtained from the considerations of continuity of the (unreversed) particle velocity and uniform static stress drop over the rupture area.

The success of this kinematic description in duplicating Madariaga's (1976) results has encouraged us to attempt to describe asymmetric stopping mechanisms in a similar manner. However, the analytic complexities of an asymmetrical rupture model preclude an explicit use of the second criterion, i.e., the uniform static stress drop. We have weakened this constraint to the more realistic constraint of $\Delta\sigma(\underset{\sim}{\xi}) \geq \tau_e$ over the rupture area. In our asymmetrical model, the healing at any point is described by a general analytic form for the particle velocity,

$$\Delta\dot{u}_h(\underset{\sim}{\xi},t) = \frac{A(\underset{\sim}{\xi})(T_h(\underset{\sim}{\xi})-t)t}{(T_h(\underset{\sim}{\xi})-T_s(\underset{\sim}{\xi}))(t^2-T_r^2(\underset{\sim}{\xi}))^{\frac{1}{2}}} \qquad T_s(\underset{\sim}{\xi}) < t < T_h(\underset{\sim}{\xi}) \qquad (5)$$

where $T_s(\underset{\sim}{\xi})$ is the arrival time of the diffracted P-wave and $T_h(\underset{\sim}{\xi})$ is the time of healing, i.e., $\Delta\dot{u}(\underset{\sim}{\xi},t) = 0$ for $t \geq T_h(\underset{\sim}{\xi})$. Our motivation for assuming that the diffraction effect dominates the healing is derived from consideration of the causal behavior of the shear stress in our frictional model during rupture.

Behind the rupture front, the shear stress acting on the rupture surface is at the dynamic frictional stress level; the diffracted P-wave carries a negative stress pulse, dropping the shear stress below this frictional stress level such that the rupture begins to heal. As an overview, it is useful to regard the motion at an interior point as continuing until information (carried by the diffracted P-wave) concerning the finiteness of the fault reaches it and healing begins. The kinetic energy of the fault motion is dissipated in frictional heating, while the negative stress pulses of the waves diffracted from the rupture stopping lower the loading stress in a monotonic fashion, so that the final static stress level is lower than the dynamic frictional stress, by which we obtain $\Delta\sigma(\underset{\sim}{\xi}) \geq \tau_e$. In stress release models where the dynamic frictional stress is zero, the slip reverses itself, oscillating around a static offset with the uniform stress drop τ_e (the loading stress), and the kinetic energy is radiated seismicly (Burridge, personal communication).

STOPPING BEHAVIOR

For our analytic specification of the particle velocity over the fault surface, we need only determine the three times; $T_r(\underset{\sim}{\xi})$, $T_s(\underset{\sim}{\xi})$ and $T_h(\underset{\sim}{\xi})$ for each grid point within the rupture area. As a first approach, we have set $T_s(\underset{\sim}{\xi}) = T_h(\underset{\sim}{\xi}) - \overline{st}$ where $\overline{st}$ is the stopping or healing interval for the particle motion at all points on the fault. This constant healing interval for the entire rupture area, combined with a constant rupture velocity, v, produces a fault perimeter of width,

$$\Delta r = \overline{st}\left(\frac{av}{v+a}\right)$$

over which the particle velocity is "smoothed", i.e.,

$$\Delta\dot{u}_h(\underset{\sim}{\xi},t) = \frac{A(\underset{\sim}{\xi})(T_h(\underset{\sim}{\xi})-t)t}{\overline{st}(t^2-|\underset{\sim}{\xi}|^2/v^2)^{\frac{1}{2}}} \qquad |\underset{\sim}{\xi}|/v^2 < t < T_h(\underset{\sim}{\xi}) \qquad (6)$$

producing an excellent approximation of a rupture which stops gradually, in the manner of the D-model discussed in the September 1977 semi-annual report, but which also heals in a causal fashion. By this approach, our general specification allows us to vary Δr systematically, in order to model faults which stop in an arbitrarily gradual or sudden fashion, thereby obtaining shear wave spectra which show spectral falloffs of $2 < \gamma < 3$ and the general two corner frequency envelopes of the type discussed by Boatwright (1978). The possibility of modelling such a general class of rupture growth and stopping behaviors in a systematic fashion represents a significant advance in source modelling. Although the particular analytic form for this stopping is not dynamically motivated, on this perimeter the healing factor may be decomposed as

$$\frac{(T_h(\underset{\sim}{\xi})-t)}{\overline{st}} = \frac{(T_h(\underset{\sim}{\xi})-|\underset{\sim}{\xi}|/v)}{\overline{st}} \quad \frac{(T_h(\underset{\sim}{\xi})-t)}{(T_h(\underset{\sim}{\xi})-|\underset{\sim}{\xi}|/v)}\ , \qquad (7)$$

where we may identify the first term as the appropriate decrease of $A(\underset{\sim}{\xi})$ resulting from an implied decrease in rupture velocity. The second term, $(T_h(\underset{\sim}{\xi})-t)/(T_h(\underset{\sim}{\xi})-|\underset{\sim}{\xi}|/v)$, exhibits the linear healing characteristic of the interior rupture area.

As shown in the series of snapshots in Figure 3, detailing the growth of the dislocation on this fault perimeter, the interaction of the rupture growth

and healing produces a realistically smoothed distribution of slip at the fault boundary, in constrast with the D- and M-models of the September 1977 semi-annual report. The uppermost snapshots of Figures 2 and 4, i.e., the final slip distributions of the M-model and the A-model also display this difference.

Using the technique of Andrews (1974), we have calculated the static stress drop for one of the A-models, for $T_o = .4$, $x_o = .2$, $\alpha = 2.$ and $\overline{st} = .1$. The results are displayed in Figure 5. The effect of the gradual stopping is to smooth the stress drop, weakening the stress concentration at the perimeter of the fault. The peaked behavior of the stress drop at $\underset{\sim}{x}_o$ is a result of our healing specification, in particular, the fact that $\overline{st}$ is constant for the entire fault surface. A variation of $\overline{st}$ over the interior of the fault could be determined such that the stress drop was smooth in the manner of the M-model but it would have little effect on the radiated pulse shapes.

To complete our model, we need only specify $T_h(\underset{\sim}{\xi})$. In the models analysed for this report, we have used

$$T_h(\underset{\sim}{\xi}) = T_o - |\underset{\sim}{\xi} - \underset{\sim}{x}_o|/\alpha$$

where T_o is the time from the nucleation to the complete healing of the rupture, and $\underset{\sim}{x}_o$ defines the direction and relative extent of the asymmetry of the final rupture area. The rupture area generated by the interaction of the circular growth and this (offset) circular healing is approximately elliptical, with eccentricity $.4 < e < 1.0$. The specific form of the healing may be easily varied to produce whatever final rupture area, relative to the point of nucleation, desired. In Figure 4 we show snapshots at equal time intervals ($\Delta t = .1$) of the growth and healing of the A-model. The parts of the fault which are healing are shown darkened.

RESULTS

One significant feature of these "pseudo-dynamic" models is that the seismic energy radiated is consistent with the theoretical analysis of Kostrov (1974) and Madariaga (1976) for general frictional models of rupture. This allows us to use both the energy flux pulse shapes and the time-integrated energy flux of the body wave arrivals as realizable model constraints. The energy flux in a body wave travelling with velocity $c(\underset{\sim}{x})$ is given by

$$\dot{\varepsilon}_c(\underset{\sim}{x},t) = \rho(\underset{\sim}{x})c(\underset{\sim}{x})\dot{u}^2(\underset{\sim}{x},t)$$

where $\rho(\underset{\sim}{x})$ is the density and $u(\underset{\sim}{x},t)$ is the ground displacement. To detail this energy flux, we have included plots of the square of the ground velocity (v^2-plots) in the figures describing our model results, as they provide a particularly useful insight into the variation of the pulse shapes over the focal sphere. In Figure 7 we show the far-field shear wave radiation from a circular version of the A-model, using $T_o = .6$, $\alpha = 2.$, $v = 1.0$, and $\overline{st} = .15$, for three different takeoff angles. Our source receiver geometry is presented in Figure 6. These results provide a check of the program code, corroborating the earlier results form the M- and D-models. The shifting of the dominant contribution to the energy flux from the stopping phase to the nucleation phase as the angle between the fault normal and the direction to the observer increases is eloquently demonstrated by the variation of the v^2-plots.

The noise level produced in these computations, generally evident in the highest spectral octave, comes from the relatively coarse sampling of the stopping behavior. This level, approximately constant for each model, is easily decreased by using a finer grid.

In Figures 8-10 we present the S-waves from the model whose displacement at different intervals in time is presented in Figures 3 and 4. For this model we have used $T_o = .5$, $x_o = .4$, $\alpha = 2.$, $v = 1.$, and $\overline{st} = .1$. The resulting rupture area is elliptical, with eccentricity $e = .55$. This represents a somewhat extreme version of the A-model, but it serves to illustrate very clearly the effect on the pulse shapes of the asymmetrical healing. In Figures 8 and 9 we show the pulse shapes and spectra for six takeoff angles in a plane normal to the fault plane, starting from the direction of the rupture growth. For a rupture velocity of .98 these angles (θ_x) are respectively 15°, 45°, 75°, 105°, 135°, 165° from the direction $\underset{\sim}{x}_o$. The pulse shapes are most compact near $\theta = 40°$. This result is in contrast to the circular models, whose pulse shapes were most compact in the direction normal to the fault plane. The A-model naturally provides an intermediate form between the circular models and a unilateral model of rupture, in the manner of the Savage (1966) model. Since the A-model does not assume that the source time function for the particle velocity is identical at each point on the fault plane, the variation of the pulse shapes and spectra over the focal sphere is more pronounced.

Finally, in Figure 10, we have plotted the pulse shapes and spectra for three takeoff angles in a plane normal to the fault plane but 60° from the direction of $\underset{\sim}{x}_o$. The displacement pulse shapes at this azimuth show an intermediate behavior and a characteristic "flattened" aspect.

The radiated seismic energy is strongly focussed in the $\underset{\sim}{x}_o$ direction, such that the time integrated energy flux in the shear waves varies by a factor of twenty over the focal sphere. Further analytical work is necessary to obtain the total radiated seismic energy from the A-model, as the one-dimensional curve fitting and integration used for the circular models cannot be used here. The pronounced variation of $\varepsilon_c(\underset{\sim}{x})$, the time integrated energy flux, makes calculation of $\varepsilon_c(\underset{\sim}{x})$ an even more useful discriminant for earthqauke modelling.

CONCLUSIONS

We have shown that it is possible to build dynamically consistent models of rupture which heal in a causal and asymmetric fashion, and have generated a simple computational code by which it is possible to model a very general class of rupture growth and stopping behaviors. This A-model is similar to Savage's elliptical model, but is dynamically feasible. We have computed pulse shapes and spectra for a particular form of our model, having a 70% unilateral component of rupture. The displacement pulse shapes, v^2-pulse shapes and integrated energy flux vary substantially over the focal sphere, providing the seismologist with a series of discriminants for the modelling of seismically recorded earthquakes. We plan to use this model extensively in order to interpret several large, multiply recorded aftershocks of the 1975 Oroville, California earthquake.

REFERENCES

Achenbach, J.D., Ray method for elastodynamic radiation from a slip zone of arbitrary shape, J. Geophys. Res., 1978 (in press).

Andrews, D.J., Evaluation of static stress on a fault plane from a Green's function, Bull. Seism. Soc. Am., 64, 1629-1633, 1974.

Andrews, D.J., Rupture progagation with finite stress in antiplane shear, J. Geophys. Res., 81, 3575-3582, 1976a.

Andrews, D.J., Rupture velocity of plane strain shear cracks, J. Geophys. Res., 81, 5679-5687, 1976b.

Boatwright, J., Detailed spectral analysis of two small New York State earthquakes, Bull. Seism. Soc. Am., 1978 (in press).

Brune, J.N., Tectonic stress and the spectra of seismic shear waves from earthquakes, J. Geophys. Res., 75, 4997-5009, 1970.

Burridge, R., Admissible speeds for plane-strain self-similar shear cracks with friction but lacking cohesion, Geophys. J. R. astr. Soc., 35, 439-455, 1973.

Burridge, R., and G.S. Halliday, Dynamic shear cracks with friction as models for shallow focus earthquakes, Geophys. J. R. astr. Soc., 25, 261-283, 1971.

Dahlen, F.A., On the ratio of P-wave to S-wave corner frequencies for shallow earthquake sources, Bull. Seism. Soc. Am., 64, 1159-1180, 1974.

Kostrov, B.V., Seismic moment and energy of earthquakes, and seismic flow of rock, Izv. Fizika Zemli, 1, 23-40, 1974.

Madariaga, R., Dynamics of an expanding circular fault, Bull. Seism. Soc. Am., 66, 639-666, 1976.

Madariaga, R., Implications of stress drop models of earthquakes for the inversion of stress drop from seismic observations, Pure and Applied Geophys., 1977 (in press).

Richards, P.G., The dynamic field of a growing plane elliptical shear crack, Int. J. Solids Structures, 9, 843-861, 1973.

Savage, J.C., Radiation from a realistic model of faulting, Bull. Seism. Soc. Am., 56, 577-592, 1966.

Savage, J.C., Relation of corner frequency of fault dimensions, J. Geophys. Res., 77, 3788-3795, 1972.

FIGURE CAPTIONS

Figure 1: Generalized plot of the particle velocity at an arbitrary point on the fault surface. T_r denotes the arrival of the rupture front, T_s the arrival of a "stopping phase" diffracted from the edge of the fault, and T_h is when the rupture heals.

Figure 2: Snapshots, at equal time intervals, of the particle displacement for the M-model. In the first three time intervals, it is growing in a self-similar fashion, while by the forth snapshot, it has stopped and is beginning to heal. The shaded region marks where the rupture surface is healing, in transition from the (unshaded) region of self-similar growth inside the healing rings to the (unshaded) region where the fault is healed. The uppermost graph shows the final slip distribution.

Figure 3: Detail of the stopping behavior of the A-model shown in Figure 4. The healing regions are shown darkened. Note how the rupture "smooths" as it reaches the final fault perimeter.

Figure 4: Snapshots of the particle displacement for the full A-model. The rupture growth is 70% unilateral. The healing region is generated by a stopping event to the left of the point of nucleation; it divides the self-similar region on the right from the healed region on the left. The uppermost graph shows the final slip distribution.

Figure 5: Static stress and displacement plots for the A-model, computed using the technique of Andrews (1974).

Figure 6: Source-receiver geometry for Figures 7-10. Σ is the fault plane ($\theta = 0$) and $\underset{\sim}{x}_0$ is the direction of rupture propagation in our asymmetrical models.

Figure 7: Pulse shapes, v^2-plots and velocity spectra for a circular version of the A-model. For a rupture velocity of $v = .9\beta$, the three takeoff angles represented here are 15°, 45° and 75° from the normal to the fault plane. Note the marked variation of the v^2-plots and the rate of spectral falloff for the three directions.

Figure 8: Pulse shapes, v^2-plots and velocity spectra for the version of the A-model whose growth and healing is shown in Figures 3 and 4. For a rupture velocity of $v = .9\beta$, these three directions are at angles of 15°, 45° and 75° from the direction of rupture, in a plane normal to the fault.

Figure 9: Pulse shapes, v^2-plots and velocity spectra for three directions (at angles of 105°, 135° and 165°) from the direction of rupture, in the same plane as Figure 6. Note the decrease in radiated energy in the back azimuths.

Figure 10: Pulse shapes, v^2-plots and velocity spectra for three directions (15°, 45° and 75°) from the normal to the fault plane, in a plane 60° to direction of rupture. Notice the flattened aspect of the pulse shapes.

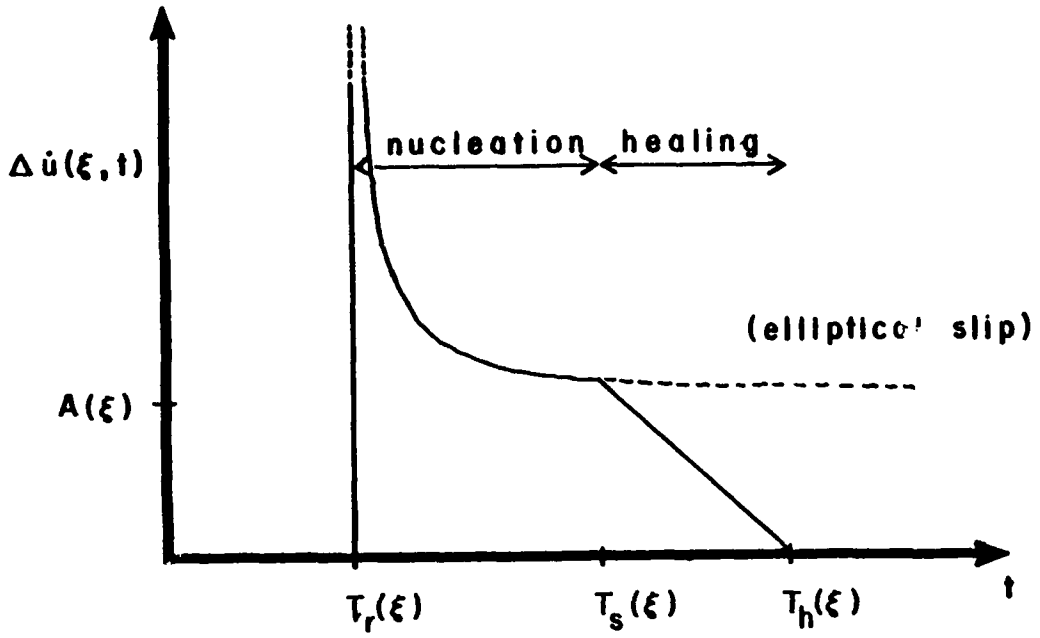
Δu̇(ξ,t)
nucleation
healing
(elliptical slip)
A(ξ)
t
$T_r(\xi)$
$T_s(\xi)$
$T_h(\xi)$

Figure 1

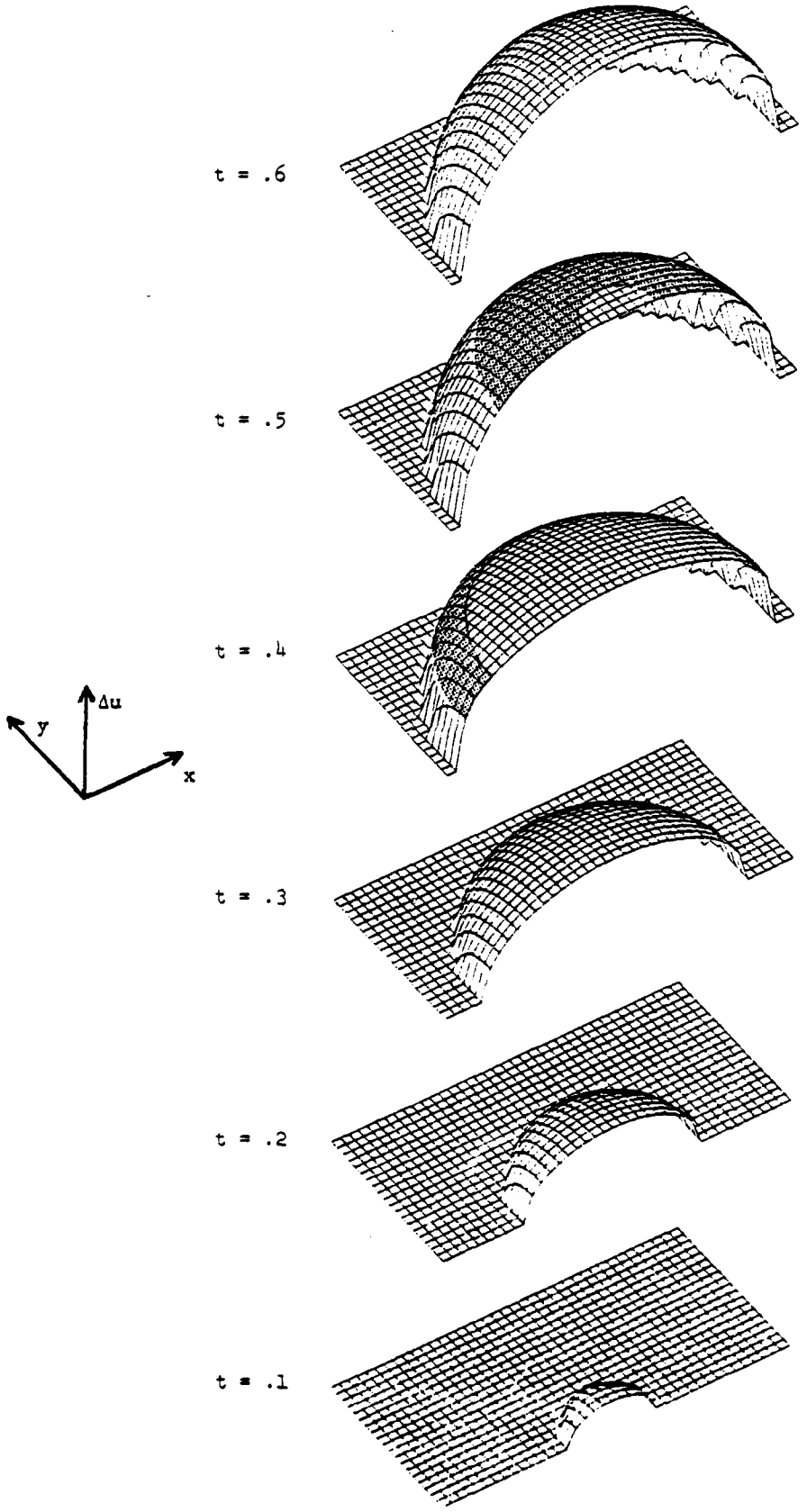

Figure 2

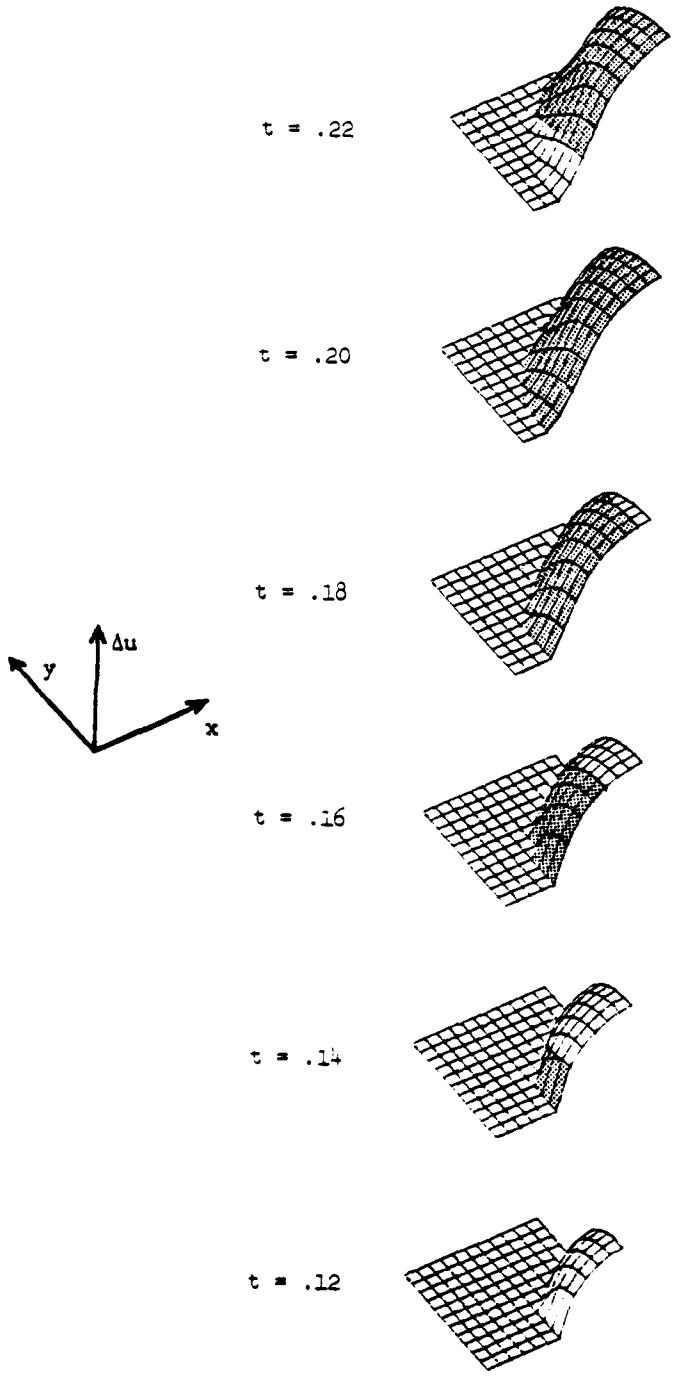

Figure 3

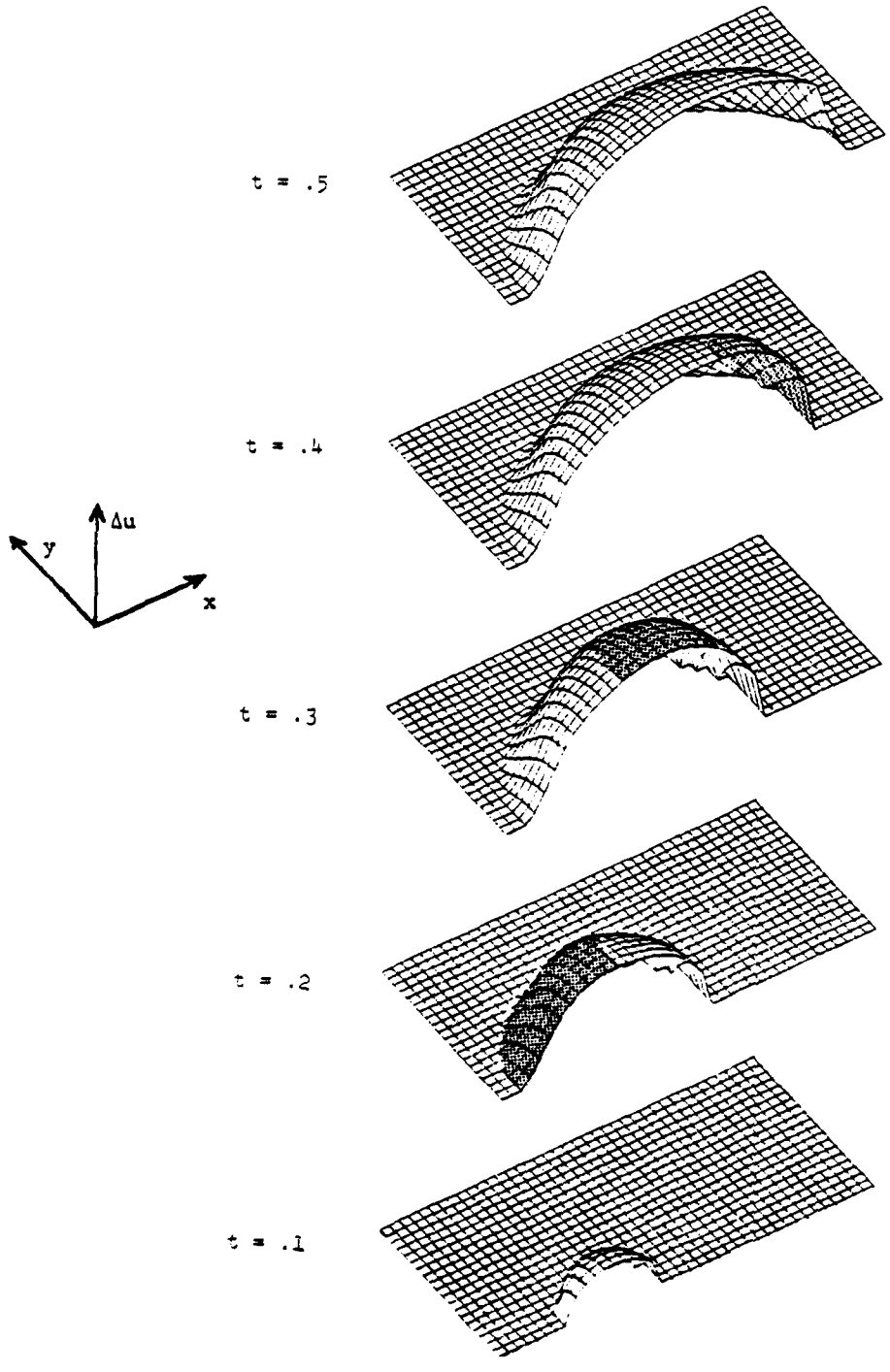

Figure 4

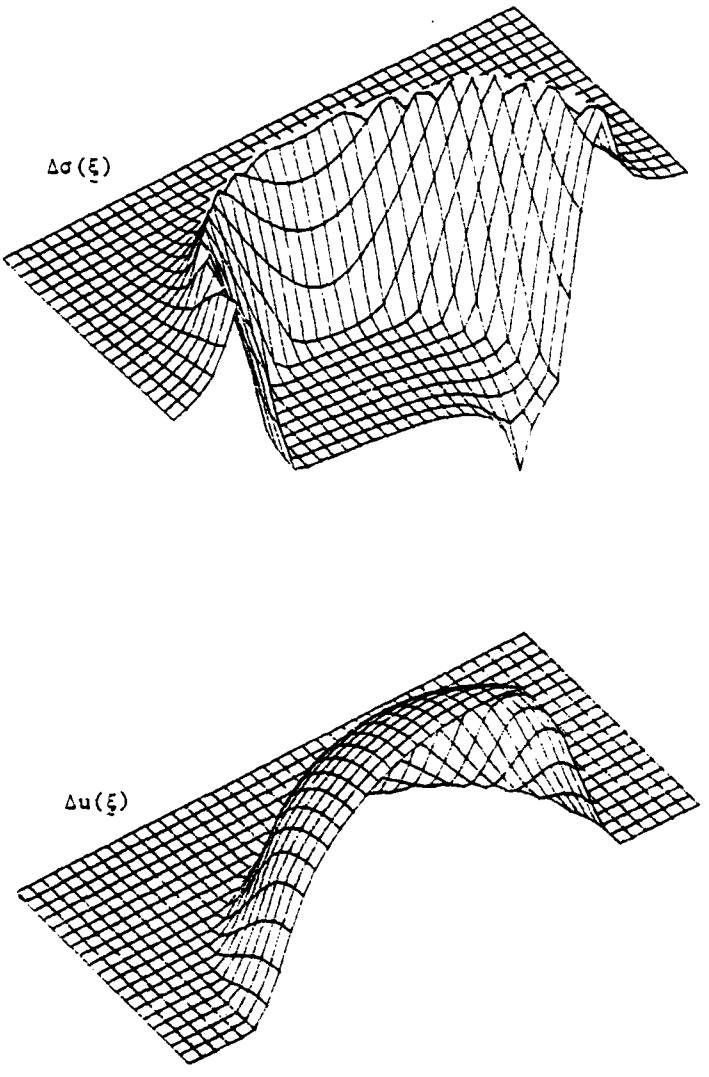

Figure 5

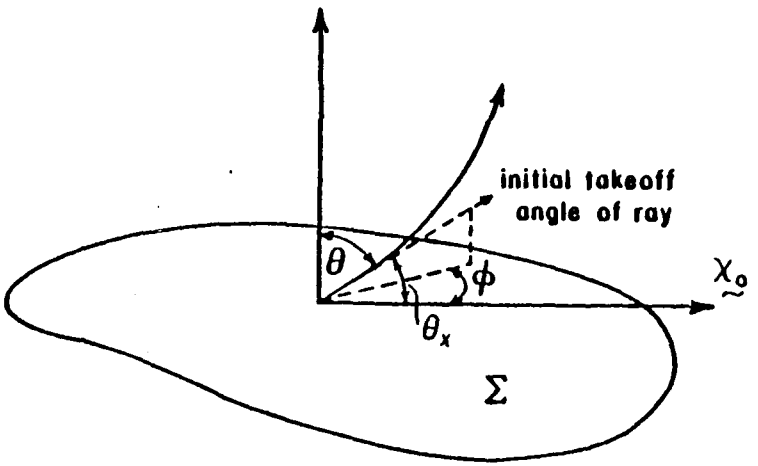

Figure 6

θ = 75°

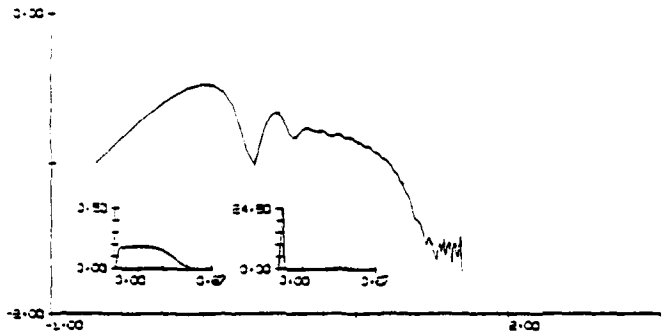

θ = 45°

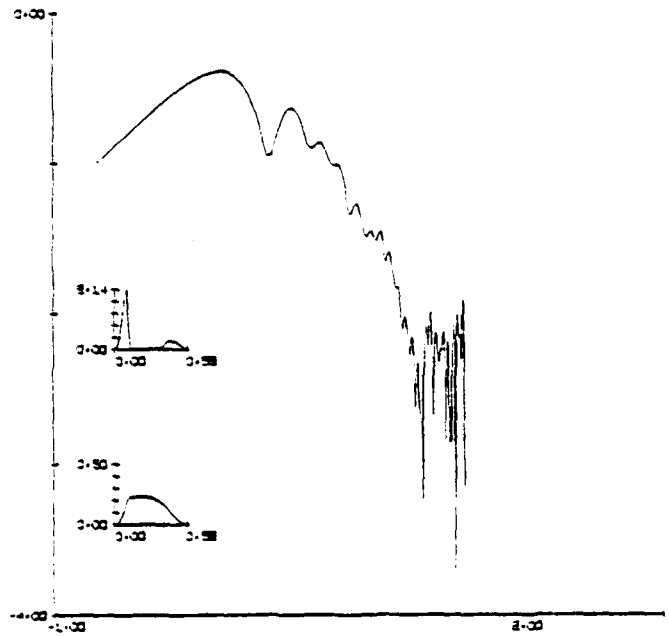

θ = 15°

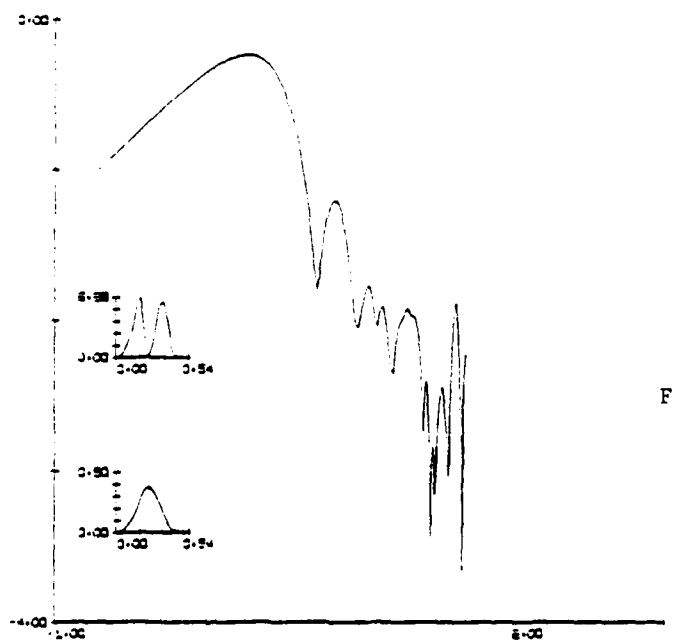

Figure 7

$\phi = 0^\circ$
$\theta = 15^\circ$
$\theta_x = 75^\circ$

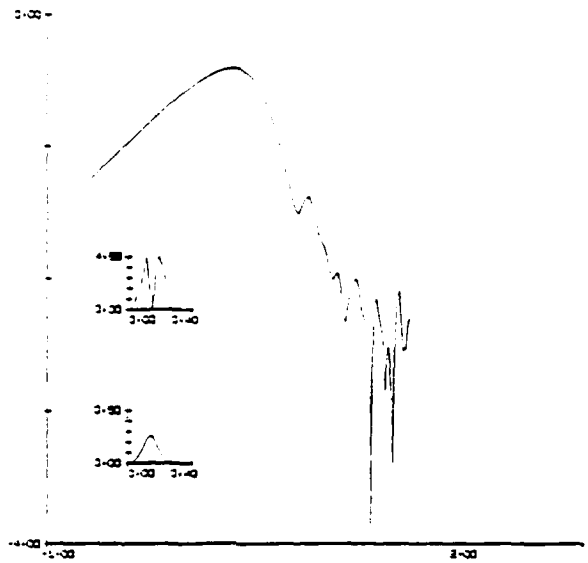

$\phi = 0^\circ$
$\theta = 45^\circ$
$\theta_x = 45^\circ$

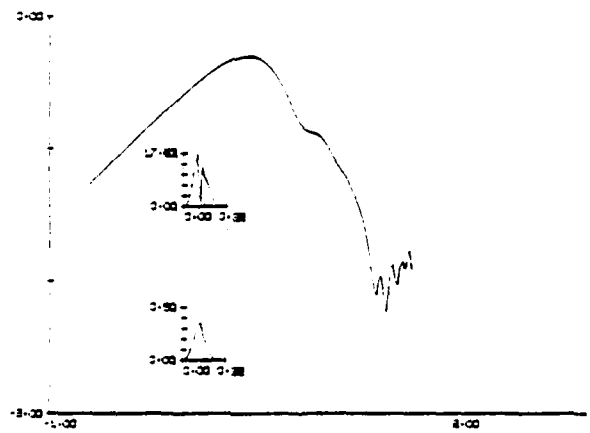

$\phi = 0^\circ$
$\theta = 75^\circ$
$\theta_x = 15^\circ$

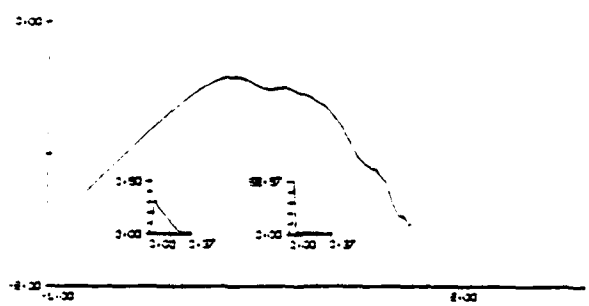

Figure 8

$\phi = 180^{\circ}$
$\theta = 75^{\circ}$
$\theta_x = 165^{\circ}$

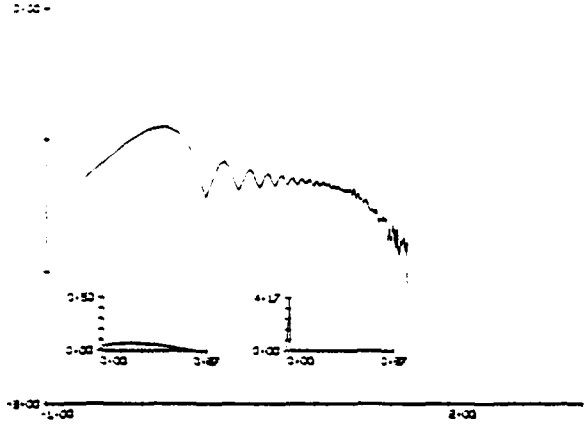

$\phi = 180^{\circ}$
$\theta = 45^{\circ}$
$\theta_x = 135^{\circ}$

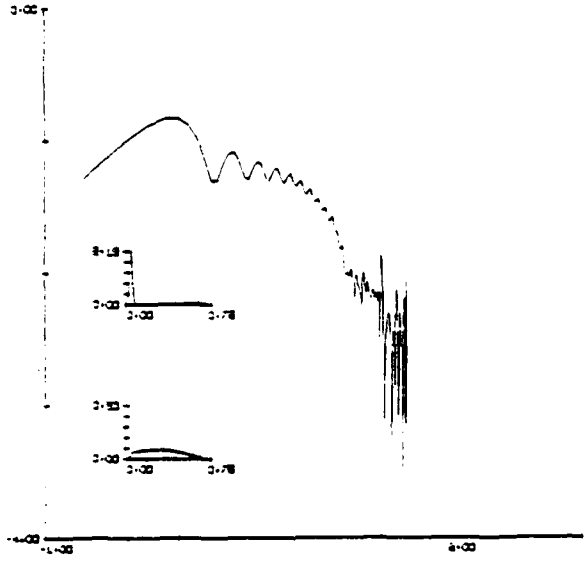

$\phi = 180^{\circ}$
$\theta = 15^{\circ}$
$\theta_x = 105^{\circ}$

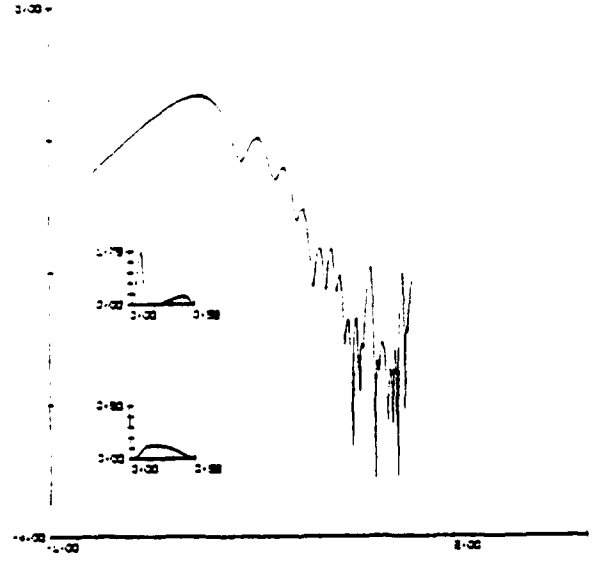

Figure 9

$\phi = 60^\circ$
$\theta = 75^\circ$
$\theta_x = 61^\circ$

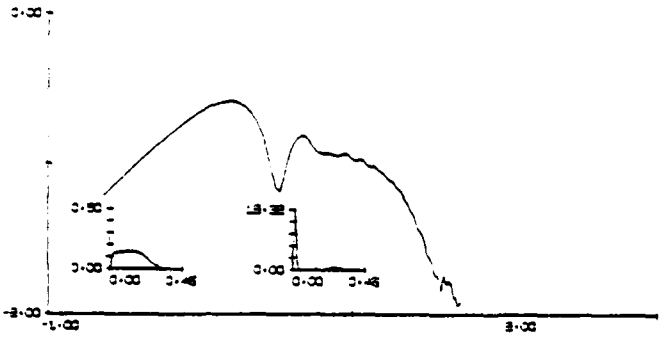

$\phi = 60^\circ$
$\theta = 45^\circ$
$\theta_x = 69^\circ$

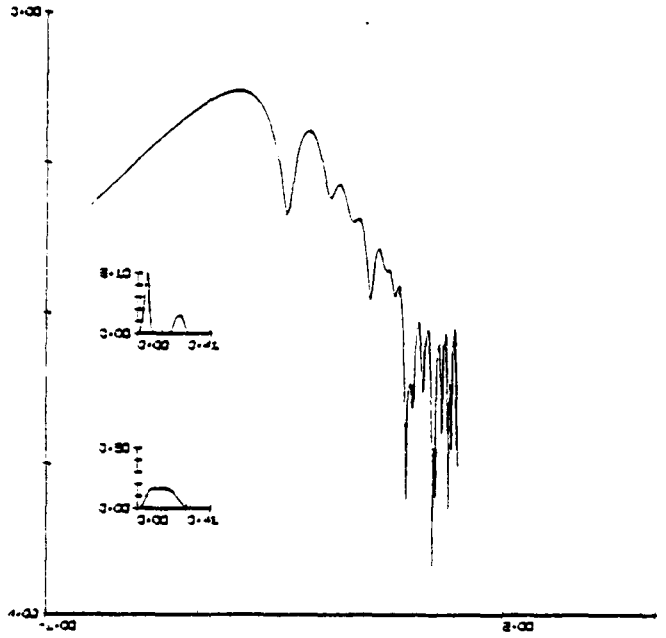

$\phi = 60^\circ$
$\theta = 15^\circ$
$\theta_x = 82^\circ$

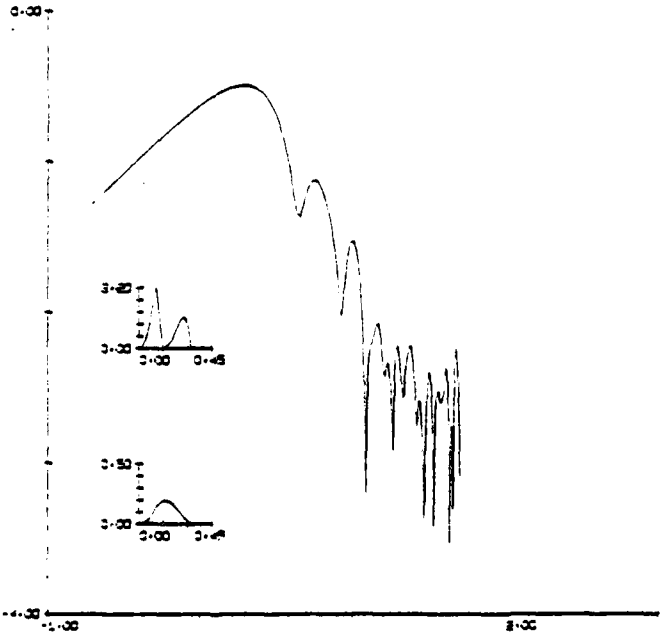

Figure 10